ELSEVIER

Surface Science 316 (1994) 103–111

surface science

Two-dimensional state resolved imaging after UV-laser induced desorption: NO/NiO(111)

M. Menges [a], B. Baumeister [a], K. Al-Shamery [a], H.-J. Freund [a,*], C. Fischer [b], P. Andresen [c]

[a] *Lehrstuhl für Physikalische Chemie I, Ruhr-Universität Bochum, Universitätsstrasse 150, 44780 Bochum, Germany*
[b] *Max-Planck-Institut für Strömungsforschung Göttingen, Bunsenstrasse 10, 37037 Göttingen, Germany*
[c] *Fakultät für Physik, Universität Bielefeld, Universitätsstrasse 25, 33615 Bielefeld, Germany*

Received 29 March 1994; accepted for publication 16 May 1994

Abstract

We present an experimental set-up which can image state selectively the two-dimensional angular distribution of neutrals or ions desorbing from a surface after UV-laser excitation together with the velocity flux distribution of a single rovibronic state in a single experiment. The method combines a state selective detection method like resonance enhanced multiphoton ionization (REMPI) with an imaging technique. This method is particularly fast in comparison to other one-dimensional methods and ideal for systems where the substrate is modified via irradiation with laser light. The normally used set-up in state resolved laser desorption experiments for two-dimensional imaging [1] is limited to look at the azimuthal distribution. We report on results of the determination of angular distributions of NO desorbing from NiO(111) after excitation with 193 nm (6.4 eV) laser light. The velocity flux distributions also obtained are compared to former one-dimensional experiments performed in our laboratory.

1. Introduction

State resolved photochemical studies on well characterized surfaces are still in an early stage [2–10]. The most simple experiment which can be modelled in a handy way involves studies of the bond breaking of surface bonds, i.e. the desorption of small molecules. The energy dissipation after the photochemical process is partly conserved in the desorbing molecules and thus gives useful information about the dynamics of such processes.

Directional effects in desorption induced by electronic transitions have first been studied for the desorption of ions after stimulation with electrons (electron stimulated desorption ion angular distribution, ESDIAD) [11]. This method turned out to be a powerful tool for the investigation of adsorbate structures (for reviews see Refs. [12,13]) and was also extended to photo-stimulated desorption [14–17]. The most frequently used experimental set-up consists of a collector positioned opposite to the surface which can detect spatially resolved positively or negatively charged particles or, under certain conditions, electronically excited neutrals. The advantage to a channeltron mounted on a goniometer [18,19] is that the full

* Corresponding author.

SSDI 0039-6028(94)00281-D

angular information can be obtained in this 2D-imaging method in a relatively short time, in principle in a single experiment. However, there is little 2D-imaging work on the detection of desorbing neutrals in their electronic ground state. The first work made in this direction combines a resonance enhanced multiphoton ionization (REMPI) technique for state selectively ionizing the neutrals with the 2D-imaging technique in the common detection geometry [1,20,21]. The method was adopted from experiments probing the photo-fragmentation in the gas phase [22,23] and investigations on ion sputtering of neutrals from surfaces [24]. However, the set-up used is limited to look at the azimuthal distribution. In order to obtain the translational energy seperate experiments have to be done. We shall present a new experimental set-up with a different geometry which can image state selectively the two-dimensional angular distribution of neutrals desorbing from a surface after UV-laser excitation together with the velocity flux distribution of a single rovibronic state in a single experiment. In comparison to other one- or two-dimensional methods this method extracts the maximum amount of information and is ideal for systems where the substrate is modified via irradiation with laser light.

As a model system we chose NO adsorbed on NiO(111). This system is well characterized with surface science methods [25–29]. Furthermore, extended experiments using a one-dimensional method were undertaken in our laboratory [30–32] and can thus be compared to our 2D-imaging results. Due to the rather large photodesorption cross section for the excitation with UV-laser light at 6.4 eV (193 nm) the system is particularly suited to undertake state and spatially resolved studies. We shall present some preliminary results on the angular distributions of single rovibronic states and compare the velocity flux distributions simultaneously obtained from the same image to our one-dimensional experiments.

2. Experimental set-up

The laser desorption experiments carried out under ultra-high vacuum (UHV) conditions were of the pump probe type. The components used in our experiments consisted of (i) a UHV system consisting of a preparation and a main chamber with sample manipulator, (ii) an excimer laser for exciting the adsorbate/substrate system and an excimer pumped tunable dye laser for probing the desorbing molecules, (iii) a detection system with spatial resolution, and (iv) a computer system interfaced to video-digitizing electronics. Each of these components will be described individually in the following section.

2.1. Vacuum chamber and sample preparation

The UHV vacuum chamber was equipped with facilities for low energy electron diffraction (LEED), Auger electron spectroscopy (AES), X-ray photoelectron spectroscopy (XPS), quadrupole mass spectrometry for residual gas analysis and thermal desorption spectroscopy (TDS), and an annex designed for the laser induced processes which we shall describe in detail further below. Except for the detector designed for the two-dimensional imaging studies [33] details of the system were discussed elsewhere [34]. The Ni(111) sample was cleaned via sputtering with Ne ions followed by annealing to 1000 K via electron bombardment. The well ordered and well characterized [25–29] epitaxial film of 4–5 layers thickness was grown by oxidizing the crystal at 500 K in an atmosphere of 5×10^{-6} Torr oxygen for 40 min.

During the laser experiments the probe was cooled by liquid nitrogen to about 95 K. At this temperature a saturation coverage of 0.2–0.3 of a monolayer of NO is adsorbed. In order to keep a constant surface coverage prior to each of the pump laser pulses the sample was redosed via background pressure of 5×10^{-8} Torr in most of the experiments. In the one-dimensional measurements this background was subtracted on alternate laser shots with the aid of a boxcar integrator. The measured background signal in the two-dimensional measurements had to be taken in a separate experiment because of the different way of recording the data. The signal of these background molecules turned out to be within the electronic noise of the detector and did not contribute substantially to the main signal.

There is a small amount of laser induced photo-reaction of NO on NiO(111) changing the properties of the system as some photo-products remain on the surface. However, the amount of reaction products is less than 5% as estimated from XP-spectra and small enough to keep the experimental conditions constant within a given experiment, if one cleans the crystal before each experiment by heating it to 700 K.

2.2. Laser

The experimental set-up is shown in Fig. 1 concentrating on a schematic view of the detection area [35,36]. The desorption was initiated normal to the surface by a pulsed broad band ArF excimer laser (Lambda Physik EMG 200) ($\lambda = 193$ nm, $h\nu = 6.4$ eV) with a pulse duration of 15 ns, and a repetition rate of 4 Hz. The laser fluence typically used of 1–2 mJ/cm^2 per pulse, which leads to an estimated temperature jump of 20 K [37], was too small to initiate thermal processes. The area irradiated on the surface had a size of 20 mm^2. The desorbing molecules were probed by making use of a (1 + 1) REMPI technique. The NO molecules were excited state selectively in the first excitation step via the transitions $A^2\Sigma(v' = 0, 1, 2) \leftarrow X^2\Pi(v'' = 0, 1, 2)$ [38 + 39]. The absorption of a second photon leads to the ionization of the NO. As NO has an unpaired electron two different spectra due to the two different spin states are obtained. The necessary tunable UV light in the 220–227 nm range was generated via frequency doubling in a barium borate (BBO 1) crystal. The fundamental radiation at 440–454 nm was obtained from an excimer laser (XeCl, Lambda Physik LPX 205 i CC) pumped dye laser (Lambda Physik LPD 3002) operated with Coumarin 2 (10–15 ns pulse length, repetition rate 4 Hz).

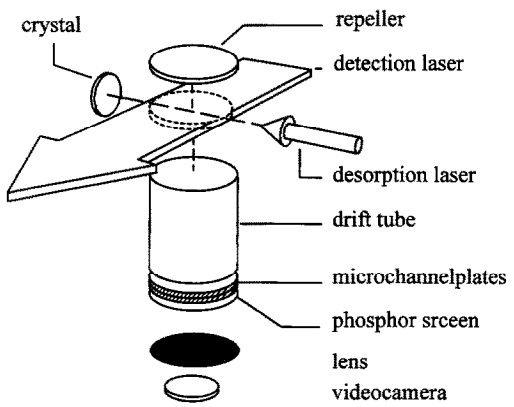

Fig. 1. Schematic drawing of the experimental set-up concentrating on a schematic view of the detection area.

2.3. Detector with spatial resolution

For imaging the desorbing species we use a detector which is normally used for example in order to measure temperature profiles in flames for molecules such as NO or OH [40–43]. In order to get the two-dimensional information the detection laser beam was widened to a sheet of 20–25 mm with the aid of a telescope consisting of two cylindrical lenses ($f = 42$ mm and $f = 310$ mm). The ions were recorded perpendicular to the surface normal and the detecting laser beam via a system consisting of a repeller (−3 kV), a drift tube of 60 mm length, multichannel plates (Galileo 3040, 40 mm diameter) and a phosphor screen (−3 kV) as depicted in Fig. 1. The distance between the crystal and the start of the detection area was 12 mm. As the MCPs are UV-light sensitive the drift tube is necessary in order to avoid signals from scattered light. The high voltage of the MCPs (+1.65 kV) was gated. It was switched on 2 μs after firing the detection laser and run for 40 μs. The flight tube consisted of a metal tube covered with meshes (wire thickness = 25 μm, mesh size = 230 μm) to obtain a field free region. The size of the flight tube was short enough so that image aberrations due to Coulomb interaction of the ions were avoided. Furthermore, an imaging dependance on the velocity of the desorbing molecules was less than 4% in the worst case, i.e. for the fastest molecules (maximal detected velocity: 1800 m/s) as obtained from calibration measurements with a pulsed molecular beam. This dynamical effect is due to the fact that the velocity components perpendicular to the component in direction to the MCPs are still existing when the molecules travel through the flight tube. It strongly depends

on the repeller voltage and length of the flight tube and was minimized by chosing the conditions given. Signal saturation effects were observed for NO pressures above 8×10^{-7} Torr, an order of magnitude above the normal working pressure. In the pressure range used the intensity of the image was linearly proportional to the amount of NO. From calibration measurements with a grid a nonlinear distortion of the electric field in the detection volume in the presence of the Ni-crystal was observed which was particularly pronounced close to the crystal (up to 10% deviations). This distortion could be completely compensated when floating the crystal at a gated potential of 1050 V. One-dimensional measurements were carried out with and without this extra potential. The velocity flux distributions from the desorbing molecules were identical in both measurements so that it was obvious that the potential did not distort the signals.

2.4. Video-digitizing system

The image on the phosphor screen was monitored through an ordinary UHV window by a CCD video-camera with a commercial objective (Pentax, $f = 50$ mm, f-number = no. 1/1.4). The camera (Theta-System HTMC87) consists of a controller (camera electronics) and a head with a CCD chip and works according to the frame-transfer principle. The CCD-chip (Thompson, TH7863FO) consisted of 288×384 light sensitive elements with an element size of 23×23 μm. The whole set-up allowed objects down to a size of 0.1 mm to be imaged. The video signal was digitized with 8-bit resolution via a video-recorder with an imaging processor card (Matrox MVP-AT) storing the data in a 512×512 pixel matrix. This recording system allows at the same time to tape the 2D-images on a video-band, to follow the signal on a RGB monitor directly and to process them via the imaging processor card with a computer. The video-electronics operated at 50 Hz and were synchronized to the working frequency of 4 Hz of the laser desorption experiments. Typically 200–500 exposures were added to obtain a single image. Due to geometric restrictions three to four images at different delay times between desorption and detection had to be taken in order to cover the whole velocity flux distribution of the desorbing molecules.

2.5. Data analysis

A typical state selective image of NO desorbing from NiO(111) is given in Fig. 2. In order to obtain the real density distribution of the desorbing molecules, first the background signal from gas phase NO had to be subtracted and then a correction concerning the laser intensity distribution within the laser sheet had to be done. For this purpose a 2D image of NO background molecules was taken without the desorption laser being switched on. An analysis of this 2D image along the surface normal gave the laser beam profile. As the REMPI signal was linearly dependent on the detection laser intensity the signal measured at the MCPs for the desorbing molecules was divided by the local laser intensity obtained from this calibration measurement.

If one wants to analyse the image in terms of the angular distribution and the velocity flux distribution of the desorbing molecules one has to take into account that the pixel coordinates of the image have to be transformed into real space coordinates. Therefore a calibration with a grid with a 2 mm spacing held into the detection laser beam was undertaken. Zones of illuminated and

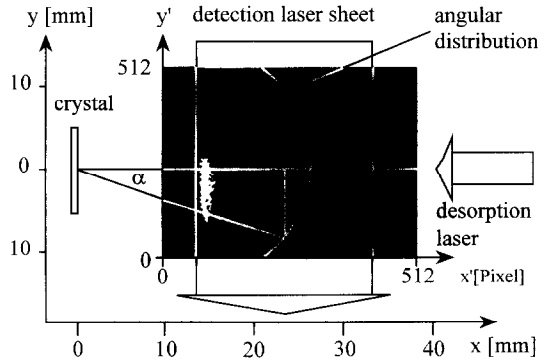

Fig. 2. 2D image of NO ($J'' = 5.5$, $v'' = 0$, $^2\Pi_{3/2}$) desorbing from NiO(111) taken at 15 μs after excitation with laser light of 6.4 eV at a distance of 12 mm; white areas correspond to the highest intensities of desorbing molecules; the image was corrected concerning background and laser beam profile.

dark parts on the image could be related to the corresponding strip pattern of the grid in real space (calibration of x-axis in Fig. 2). Another way of calibration was realized by imaging the unwidened detection laser beam on the MCPs at several known positions (calibration of y-axis in Fig. 2 by guiding the detection laser beam along or parallel to the surface normal). From this calibration a function was obtained with which any pixel coordinate could be transformed into a real space coordinate. For an analysis the intensity map was averaged over 10 pixels along the x-axis.

3. Results and discussion

3.1. Velocity flux distributions

In order to obtain the translational energy distribution of the desorbing molecules, the probe laser was fixed to the maximum of a specific rovibronic transition of the NO. The 2D image of the desorbing particles was measured at a fixed delay time between pump and probe laser. Three or four images at different delay times between desorption and detection were taken in order to cover most of the desorbing molecules. An example of such a 2D image corrected for the laser intensity distribution is shown in Fig. 2. From the 2D image in principle one can obtain the velocity flux distributions of the desorbing molecules at any desorption angle. We restricted our analysis to the distribution along the surface normal at the center of the crystal in order to be able to compare our results to one-dimensional measurements for the same molecular system. As we measure particle densities the corrected intensity distribution obtained from the 2D image has to be multiplied with the real space coordinates and the delay time between desorption and detection at which the image was taken in order to obtain the corresponding velocity flux distribution. Fig. 3 shows such an analysis for the same rovibrational state as in Fig. 2 taking three overlapping 2D images at three different delay times. As we measure a density of molecules the intensity measured has to be weighted with the time delay in order to obtain the velocity flux distribution. The minimum and maximum velocity (Δv) that can be registered in one image is therefore not only linearly depending on the expansion of the detection laser sheet (Δx) but also inversely on the delay time t_d chosen. This explains the different widths of the ranges concerning the velocities covered in the 2D images for the three different delay times in Fig. 3. The noise is particularly pronounced after the correction for the laser intensity at parts of low laser intensities of the 2D image. The laser was adjusted in such a way that the beam profile was close to a rectangular shape. The 2D images were then analysed taking only parts where the laser profile showed its maximum and was mainly flat (60% of the total image). In Fig. 3 the velocity flux distribution of the same state obtained from a one-dimensional measure-

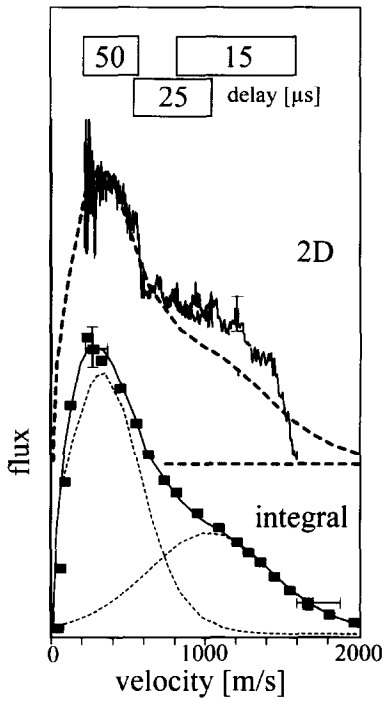

Fig. 3. Upper curve: Velocity flux distribution of NO ($J'' = 5.5$, $v'' = 0$, $^2\Pi_{3/2}$) desorbing from NiO(111) extracted from three 2D images along the surface normal (15, 25 and 50 μs after excitation with laser light of 6.4 eV). Lower curve: corresponding velocity flux distribution from a one-dimensional measurement [30–32].

ment can also be seen together with a fit of the data.

As is clearly seen, the 2D-imaging experiments verify our findings of the one-dimensional experiments that UV-laser induced desorption of NO from NiO(111) leads to bimodal velocity flux distributions [30–32]. The overall shapes of the distributions differ slightly from each other, i.e. the peaks in the one-dimensional distribution are broader, particularly for the slow channel. The uncertainty of the velocity in our 2D image is due to the diameter of the irradiated area on the surface (2.5 mm). However, the uncertainty in the one-dimensional measurement is due to the diameter of the detector (40 mm) crossed by the laser beam as molecules reaching the edge of the detection area are faster than molecules in the center. To this range of velocities only one velocity is attributed in the TOF, i.e. the slowest component which points along the surface normal. From the detection angle covered it can be estimated that the fastest molecules at the edge have a velocity 15% above the velocity along the surface normal. As a result, the velocity flux distribution is shifted with respect to the real distribution towards slower velocities. Also the detection laser beam has a finite size along the x-axis of 2 mm so that the intensity is not only measured at a single velocity but at a range of velocities covered by the finite size of the laser beam (velocity range covered: velocity in the middle of the beam $\pm 10\%$). As to this range of velocities, a single velocity is attributed and this leads to a smearing of the velocity flux distribution in the one-dimensional measurements.

3.2. Angular distributions

From 2D images like the one shown in Fig. 2, the angular distribution, i.e. the density distribution of particles with a fixed velocity as a function of the angle related to the surface normal, can be obtained. For the analysis we first choose the velocity v for which we want to extract the angular distribution. With this velocity the particle covered a distance s and can be found at a place with the coordinates x (perpendicular to the surface) and y (parallel to the surface) in real space coordinates. As the image is taken at a certain delay between pump and probe laser t_d, the following relation between coordinates in real space and velocity are obtained:

$$x = x(v, t_d, \Theta) = s\cos(\Theta) = vt_d\cos(\Theta),$$
$$y = y(v, t_d, \Theta) = s\sin(\Theta) = vt_d\sin(\Theta). \quad (1)$$

The density of particles measured with our 2D image for this particular velocity and angle can now be extracted from the image by reading out the intensity at the pixel coordinates corresponding to the real space coordinates given.

Examples for such angular distributions are shown in Fig. 4 for different velocities for the rovibronic state from Figs. 2 and 3. Due to restrictions concerning the detector, size angles between $+30°$ and $-30°$ with respect to the surface normal can be covered.

As can be seen from Fig. 4, the angular distributions of the desorbing molecules are peaking increasingly towards the direction of the surface normal with increasing velocity. This trend turns out to be general when looking at different rovibronic states. We analysed the data by fitting the distributions with $\cos^n(\Theta)$ functions. We found exponents between 1 for the molecules at $v = 250$

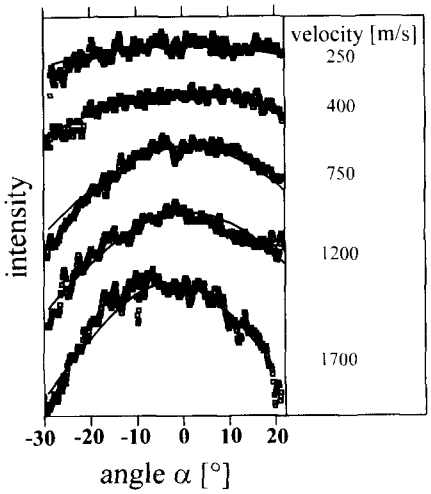

Fig. 4. Angular distributions of NO ($J'' = 5.5$, $v'' = 0$, $^2\Pi_{3/2}$) desorbing from NiO(111) extracted for different velocities from three 2D images (15, 25 and 50 μs after excitation with laser light of 6.4 eV).

m/s and 15 for $v = 1700$ m/s. However, the differences between values for high exponentials of the cosine function are only minimal so that the estimated error of the high exponentials is ± 3 due to the noise of the signal, the narrow angular range of the detection system and further errors discussed in the experimental section. This strongly peaked distribution of the fast channel means that the molecules have a fast velocity component pointing along the surface normal and only slow velocity components in the y and z directions. The strong peaking along the surface normal has also been observed in electron-stimulated desorption experiments on NO from NO_2/Pt(111) [20], CO/Pt(111) [21] or laser desorption experiments of NO/Pt(111) [44–46].

3.3. Modelling the data

The main goal of this paper is to present the experimental set-up for the 2D-imaging of the desorbing molecules and the comparison of the experimental results to one-dimensional measurements. This was done in the last two paragraphs. For those readers that are also interested in the physical meaning of our experimental results, we want to summarize only briefly the main results of model calculations undertaken in our laboratory. Details of the calculations including potential energy surfaces used have been and are going to be published elsewhere [32,36,47]. The bimodal velocity flux distributions were already found in the one-dimensional measurements and the findings of the model calculations will only be summarized. The information concerning the strongly peaked angular distributions is new and deserves a brief discussion.

Based on the Menzel–Gomer–Redhead (MGR) model [48,49] we did quasi-classical trajectory calculations on the dynamics of the laser induced process. Within the calculations the rotational motion and the electronic excitation were treated quantum mechanically while the translational motion was treated classically. Within the calculations the adsorbed state with a 45° bending geometry was treated as a hindered rotor concerning the bending vibrational motion allowing a free rotation azimuthally about the surface molecule bond. For the excited state which has the character of NO^- being bound to NiO [30–32] we assumed a Morse potential with respect to the bonding towards the surface with a minimum located at smaller molecule surface distances. Within the angle dependent part of the potential we allowed free rotation. Deactivation from the excited state occurs after a given lifetime assuming the relaxation probability being dependent on the place within the excited hypersurface.

The tilted geometry of 45° of NO on the NiO surface, respectively the motion of the center of gravity normal to the surface related to it, leads to different starting conditions for the trajectories. They depend on the sign of the component of the motion normal to the surface (k_x). On the other hand, trajectories belonging to longer lifetimes allow the molecule to reach the strongly repulsive part of the potential. This leads to high translational energies upon deactivation. Both effects are important to explain the bimodality of the velocity flux distributions.

As the potentials describe a fixed and smooth surface we kept the components of the momentum parallel to the surface of the desorbing molecules constant as can be seen in Fig. 5. The component normal to the surface was then obtained from trajectory calculations. From our calculation we obtain strongly peaked angular distributions of the fast molecules restricted to angles smaller than 40°. The calculated distributions [47] represent the experimental distributions well. With decreasing velocities normal to the surface the angular distributions broaden as found experimentally. The result means that the kinetic en-

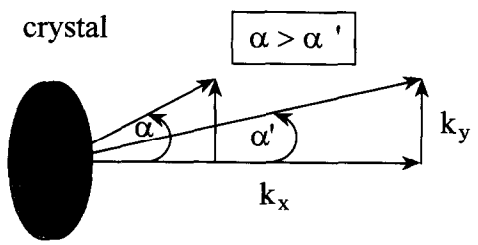

Fig. 5. Schematic drawing for the two components of the translational momentum k in the detection plane for slow and fast desorbing molecules.

ergy of the molecules gathered in the excitation process is mainly transformed during the desorption into a translational motion along the surface normal.

5. Conclusions

In contrast to the most commonly used geometry our experimental set-up for a 2D-imaging method presented in this paper allows one to obtain state selectively the two-dimensional angular distribution of desorbing neutrals together with the velocity flux distribution of a single rovibronic state in a single experiment. This is realized by positioning the detector for the desorbing molecules perpendicular to the surface plane. The state selectivity results from resonance enhanced multiphoton ionization (REMPI) with the detection laser beam being widened to a sheet parallel to the detector plane. As a model system we used NO desorbing from NiO(111) after excitation with 193 nm (6.4 eV) laser light. The velocity flux distributions obtained from our imaging method were bimodal similar to results obtained in former one-dimensional experiments performed in our laboratory. The uncertainties in determining the velocity flux distributions of the one-dimensional measurements lead to shifts in the velocity flux distributions and to a smearing of the distributions. These problems can be solved in the 2D measurements. Supplementary information can be gained in the 2D measurements concerning the angular distributions of the desorbing molecules. From the angular distribution strongly peaked for high velocities, we obtain that the molecules mainly gain kinetic energy along the surface normal during the desorption process.

Acknowledgements

We thank the Deutsche Forschungsgemeinschaft, the Ministerium für Wissenschaft und Forschung des Landes Nordrhein-Westfalen, and the Fonds der chemischen Industrie (H.-J.F.) for financial support. K. Al-Sh. thanks the Ministerium für Wissenschaft und Forschung des Landes Nordrhein-Westfalen for a Lise-Meitner Stipendium.

References

[1] (a) T.J. Chuang, R. Schwarzwald and A. Mödl, J. Vac. Sci. Technol. A 9 (1991) 1719.
(b) R. Schwarzwald, A. Mödl and T.J. Chuang, Surf. Sci. 242 (1991) 437.
[2] H. Zacharias, Appl. Phys. A 47 (1988) 37.
[3] F. Träger, in: Photothermal and Photochemical Processes at Surfaces and in Thin Films, Topics in Current Physics, Vol. 47, Ed. P. Hess (Springer, Berlin, 1989).
[4] E.J. Heilweil, R.C. Cavanagh and J.C. Stephenson, Ann. Rev. Phys. Chem. 40 (1989) 143.
[5] X.-L. Zhou, X.-Y. Zhu and J.M. White, Surf. Sci. Rep. 13 (1991) 77.
[6] R.D. Ramsier and J.T. Yates, Surf. Sci. Rep. 12 (1991) 244.
[7] Z. Rosenzweig and M. Asscher, J. Chem. Phys. 96 (1992) 4040.
[8] A.R. Burns, E.B. Stechel and D.R. Jennison, Eds., Desorption Induced by Electronic Transitions DIET V, Springer Series in Surface Science, Vol. 31 (Springer, Berlin, 1993).
[9] R.R. Cavanagh, D.S. King, J.C. Stephenson and T.F. Heinz, J. Phys. Chem. 97 (1993) 786.
[10] E. Hasselbrink, in: Laser Spectroscopy and Photochemistry on Metal Surfaces, Eds. H.L. Dai and W. Ho, in press.
[11] (a) J.J. Czyzewski, T.E. Madey and J.T. Yates, Phys. Rev. Lett. 32 (1974) 777.
(b) T.E. Madey, J.J. Czyzewski and J.T. Yates, Surf. Sci. 49 (1975) 465.
[12] (a) D. Menzel, Angew. Chemie 82 (1970) 263.
(b) D. Menzel, Nucl. Instrum. Methods Phys. Res. B 13 (1986) 507.
(c) D. Menzel, in: The Structure of Surfaces II, Eds. J.F. van der Veen and M.A. van Hove (Springer, Berlin, 1988).
[13] P. Avouris and R.E. Walkup, Ann. Rev. Phys. Chem. 40 (1989) 173.
[14] J.F. van der Veen, F.J. Himpsel, D.E. Eastman and P.J. Heimann, Solid State Commun. 36 (1980) 99.
[15] T.E. Madey, R. Stockbauer, F. van der Veen and D.E. Eastman, Phys. Rev. Lett. 45 (1980) 187.
[16] H.A. Engelhardt, W. Bäck, D. Menzel and H. Liebl, Rev. Sci. Instrum. 52 (1981) 835.
[17] H.A. Engelhardt, A. Zartner and D. Menzel, Rev. Sci. Instrum. 52 (1981) 1161.
[18] H. Niehus and B. Krahl-Urban, Rev. Sci. Instrum. 52 (1981) 56.
[19] R. Jaeger and D. Menzel, Surf. Sci. 93 (1980) 71.
[20] A.R. Burns, Surf Sci. 280 (1993) 349.

[21] A.R. Burns, E.B. Stechel and D.R. Jennison, in: Ref. [8] p. 173.
[22] D.W. Chandler, J.W. Thoman Jr., M.H.M. Janssen and D.H. Parker, Chem. Phys. Lett. 156 (1989) 151.
[23] D.H. Parker, Z.W. Wang, M.H.M. Janssen and D.W. Chandler, J. Chem. Phys. 90 (1989) 60.
[24] P.H. Kobrin, G.A. Schick, J.P. Baxter and N. Winograd, Rev. Sci. Instrum. 57 (1986) 1354.
[25] H.-J. Freund, H. Kuhlenbeck and M. Neumann, in: Adsorption on Ordered Surfaces of Ionic Solids and Thin Films, Springer Series in Surface Science, Vol. 33, Eds. H.-J. Freund and E. Umbach (Springer, Berlin, 1993) p. 136.
[26] D. Cappus, D. Ehrlich, B. Dillmann, C. Xu, C.A. Ventrice, K. Al-Shamery, H. Kuhlenbeck and H.-J. Freund, Chem. Phys. 177 (1993) 533.
[27] D. Cappus, M. Menges, C. Xu, D. Ehrlich, B. Dillmann, C.A. Ventrice, J. Libuda, M. Bäumer, S. Wohlrab, F. Winkelmann, H. Kuhlenbeck and H.-J. Freund, J. Electron. Spectrosc. Relat. Phenom. 68 (1994) 347.
[28] F. Winkelmann, S. Wohlrab, J. Libuda, M. Bäumer, D. Cappus, M. Menges, K. Al-Shamery, H. Kuhlenbeck and H.-J. Freund, Surf. Sci. 307–309 (1994) 1148.
[29] F. Rohr, K. Wirth, J. Libuda, D. Cappus, M. Bäumer and H.-J. Freund, to be published.
[30] (a) Th. Mull, H. Kuhlenbeck, G. Odöfer, R.M. Jaeger, C. Xu, B. Baumeister, M. Menges, G. Illing, H.-J. Freund, D. Weide and P. Andresen, in: Desorption Induced by Electronic Transitions, DIET IV, Springer Series in Surface Science, Vol. 19 Eds. G. Betz and P. Varga (Springer, Berlin, 1993) p. 143.
(b) M. Menges, B. Baumeister, K. Al-Shamery, B. Adam, Th. Mull, H.-J. Freund, C. Fischer, D. Weide and P. Andresen, in: Ref. [8] p. 275.
[31] K. Al-Shamery, I. Beauport, B. Baumeister, Th. Klüner, Th. Mull, M. Menges, C. Fischer, H.-J. Freund, P. Andresen, J. Freitag and V. Staemmler, Proceedings of the SPIE'S OE/Laser '94 Conference, in press.
[32] M. Menges, B. Baumeister, K. Al-Shamery, H.-J. Freund, C. Fischer and P. Andresen, J. Chem. Phys., to be published.
[33] C. Fischer, PhD Thesis, Göttingen, 1993.
[34] Th. Mull, M. Menges, B. Baumeister, G. Odöfer, H. Geisler, G. Illing, R.M. Jaeger, H. Kuhlenbeck, H.-J. Freund, D. Weide, U. Schüller, P. Andresen, F. Budde, P. Ferm, V. Hamza and G. Ertl, Phys. Scr. 41 (1990) 134.
[35] Th. Mull, M. Menges, B. Baumeister, B. Adam, K. Al-Shamery, H.-J. Freund, D. Weide, C. Fischer and P. Andresen, in: Proceedings of the 5th Symposium on Surface Science, 15–21 March 1992, France, Eds. M. Alnot, J.J. Ehrhardt, C. Launois, B. Mutaftschiev and M.R. Tempère, p. 258.
[36] Th. Mull, B. Baumeister, M. Menges, H.-J. Freund, D. Weide, C. Fischer and P. Andresen, J. Chem. Phys. 96 (1992) 7108.
[37] J.H. Bechtel, J. Appl. Phys. 46 (1975) 1585.
[38] G. Herzberg, Molecular Spectra and Molecular Structure: Spectra of Diatomic Molecules, (Van Nostrad Reinhold Company, New York, 1950).
[39] (a) D.C. Jacobs and R.N. Zare, J. Chem. Phys. 85 (1986) 5457.
(b) D.C. Jacobs, R.J. Madix and R.N. Zare, J. Chem. Phys. 85 (1986) 5469.
[40] P. Andresen, A. Bath, W. Gröger, H.W. Lülf, G. Meijer and J.J. ter Meulen, Appl. Opt. 27 (1988) 365.
[41] P. Andresen, G. Meijer, H. Schlüter, H. Voges, A. Koch, W. Hentschel and E. Rothe, Appl. Opt. 29 (1990) 2392.
[42] A.M. Wodtke, L. Hüwel, H. Schlüter, G. Meijer, P. Andresen and H. Voges, Opt. Lett. 13 (1988) 910.
[43] I.P. Csorba, Image Tubes (Howard W. Sams, Indianapolis, 1985).
[44] F. Budde, A.V. Hamza, P.M. Frem, G. Ertl, D. Weide, P. Andresen and H.-J. Freund, Phys. Rev. Lett. 60 (1988) 1518.
[45] S.A. Buntin, L.J. Richter, R.R. Cavanagh and D.S. King, Phys. Rev. Lett. 61 (1988) 1321.
[46] S.A. Buntin, L.J. Richter, D.S. King and R.R. Cavanagh, J. Chem. Phys. 91 (1989) 6429.
[47] (a) B. Baumeister, PhD Thesis, Bochum, 1994.
(b) B. Baumeister and H.-J. Freund, submitted.
(c) Th. Klüner, B. Baumeister, H.-J. Freund, J. Freitag and V. Staemmler, paper in preparation.
[48] D. Menzel and R. Gomer, J. Chem. Phys. 41 (1964) 3311.
[49] P.A. Redhead, Can. J. Phys. 42 (1964) 886.